NJC

PAPER

View Article Online
View Journal

Cite this: DOI: 10.1039/c7nj01525a

Experimental and DFT studies of disubstituted 2-(2-hydroxyphenyl)benzothiazole-based fluorophores synthesized by Suzuki coupling†

Yahui Niu,[a] Qin Wang,[a] Haoran Wu,[b] Yuxiu Wang[a] and Yanrong Zhang *[a]

Among the various fascinating fluorescent compounds, excited-state intramolecular proton transfer (ESIPT) dyes have been drawing much attention due to their anomalously large Stokes shifts. Furthermore, ESIPT fluorophores are attractive as their fluorescence properties may be fine-tuned through facile chemical modifications of existing dyes. Varying the strength of the electron-donating and electron-withdrawing substituents anchored at different sites of the parent molecules, especially when incorporating these substituents at several different sites simultaneously, is an effective way to achieve targeted fluorescence properties. In the present study, a new family of 2-(2-hydroxyphenyl)benzothiazole (HBT)-based disubstituted derivatives, with substitutions at the 4′- and 5′-positions, were readily synthesized by the Suzuki coupling reaction. It was found that the electronic effects of the 5′-position substituents on the molecular orbital levels were opposite to that of the 4′-position substituents. Theoretical calculations demonstrate that the substituents at the 4′- and 5′-positions dramatically affect the HOMOs and the LUMOs, respectively, which is in conformity with experimental results and can be applied to predict shifts in fluorescence emission. Additionally, these derivatives show highly efficient keto-emission in the aggregated state. The X-ray crystallographic analysis shows that weak intramolecular interactions, which restrict intramolecular rotation, and strong intramolecular hydrogen bonding, which facilitates intramolecular proton transfer, are responsible for the intense keto-emission observed. Our study may provide experimentally and theoretically valuable instructions for designing other high-performance ESIPT fluorophores to meet the demands of specific applications.

Received 6th May 2017,
Accepted 30th July 2017

DOI: 10.1039/c7nj01525a

rsc.li/njc

Introduction

Fluorescence is one of the fundamental properties that brings about interesting molecular functions of organic compounds. Among the various fascinating fluorescent compounds, excited-state intramolecular proton transfer (ESIPT)-active dyes have gained significant interest.[1,2] ESIPT is a typical photophysical process, whereby an excited-state proton is transferred from a H-bond donor to an acceptor through a pre-existing intramolecular H-bond, which produces a tautomer with a molecular structure and electronic distribution completely different from the originally excited species.[3] Consequently, compared with other ordinary dyes, ESIPT-active dyes display anomalously large Stokes shifts without self-absorption, which are desirable features for many important applications including white light-emitting materials[4] and fluorescent probes.[5]

2-(2-Hydroxyphenyl)benzothiazole (HBT) is one of the most extensively studied ESIPT-active dyes because of its simple structure and facile synthesis.[6] Diverse chemical modifications, *via* anchoring of different substituents at its various positions, are simple and effective strategies for regulating ESIPT to meet specific applications. For example, Zhao *et al.* conjugated naphthalimide and boron-dipyrromethene at the 5′-position of HBT, resulting in two derivatives with long-lived triplet excited states.[7] Wang *et al.* anchored different electron-donating amino groups at the 4′- or 5′-position of HBT, which exhibited emission colors across the entire visible spectrum.[8] These studies show that the fluorescence of HBT derivatives can be controlled by modifying the substituents. Despite this, most previous studies focused on the structural modification of HBT involving substituents at a single position. Few studies have explored simultaneous disubstitution of HBT, possibly due to a lack of practical synthetic methods. Han *et al.* introduced an electron-withdrawing trifluoromethyl group at the 4′-position and an

[a] College of Chemistry & Pharmacy, Northwest A&F University, Yangling, Shaanxi 712100, P. R. China. E-mail: zhangyr@nwsuaf.edu.cn; Tel: +86-29-87092226

[b] Innovation Experimental College, Northwest A&F University, Yangling, Shaanxi 712100, P. R. China

† Electronic supplementary information (ESI) available. CCDC 1546814. For ESI and crystallographic data in CIF or other electronic format see DOI: 10.1039/c7nj01525a

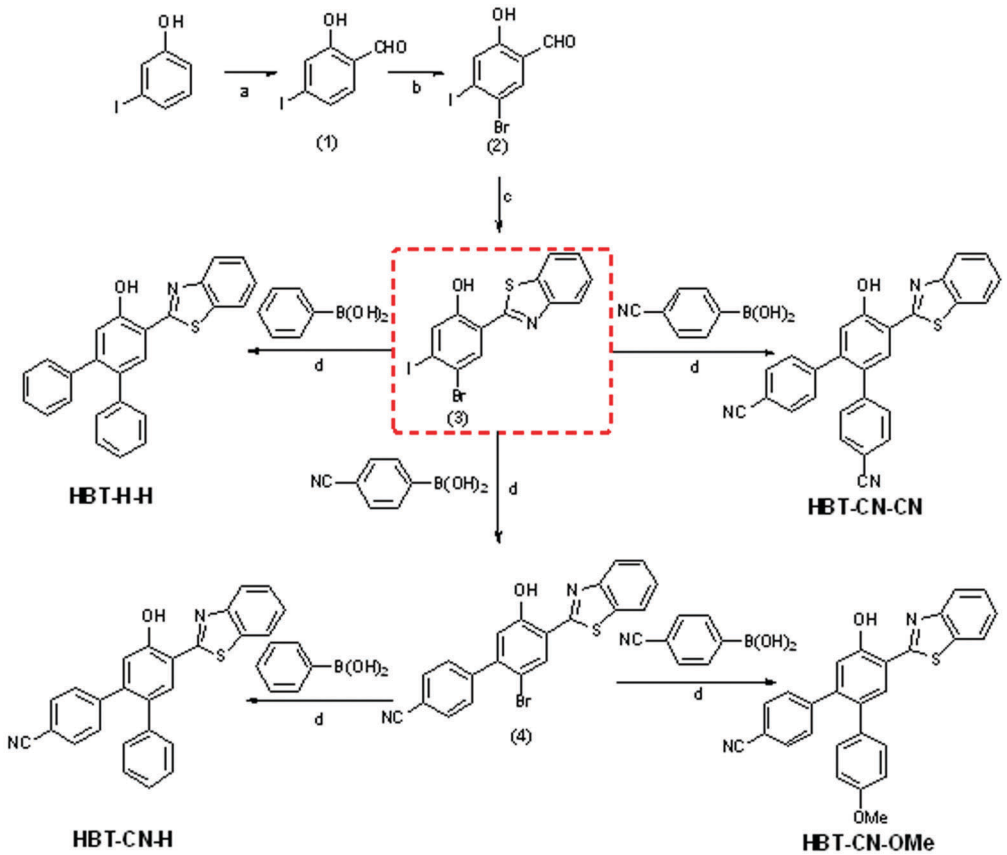

Scheme 1 Synthesis route of disubstituted HBT derivatives at its 4′ and 5′ positions. Reaction conditions: (a) (HCHO)*n*, Et_3N, $MgCl_2$, CH_3CN, reflux, 24 h; (b) AcOH, Br_2, RT, 18 h; (c) 2-aminothiophenol, 37% HCl, 30% H_2O_2/ethanol; (d) $PdCl_2(PPh_3)_2$, K_2CO_3, H_2O/dioxane, 16 h, reflux.

electron-donating triphenylamine group at the 5′-position in a single HBT derivative, which generated pure white light emission in mixed solvents.[9] In this system, the trifluoromethyl group facilitated the deprotonation of the phenolic hydroxy group, while the triphenylamine group allowed for bathochromic emission due to intramolecular charge transfer and the "red-edge effect". Therefore, exploiting the electronic effect of multiple substituents at different sites is a promising tactic in designing novel ESIPT dyes for targeted applications.

In this work, with the aim of fine-tuning the fluorescence emission properties of HBT derivatives, we designed and synthesized a new family of disubstituted HBT-based compounds by functionalizing the 4′- and 5′-positions with different substituents using Suzuki cross-coupling (molecular structures depicted in Scheme 1). Theoretical calculations, which agreed with the experimental observations, could be applied to predict the fluorescence properties of other new ESIPT dyes. On the other hand, fluorophores with aggregation-induced emission enhancement (AIEE) have shown outstanding advantages compared with those with aggregation-caused quenching in many practical applications such as chemo/biosensors[10] and OLEDs.[11] These new HBT derivatives show AIEE characteristics. The X-ray crystallographic analysis shows that weak intramolecular interactions, which restrict the intramolecular rotation, and strong intramolecular H-bonding, which facilitates proton transfer, are two important factors responsible for the intense keto-emission observed in the crystalline state.

Results and discussion

Synthesis of disubstituted HBT derivatives

To functionalize HBT with various moieties bearing different Hammett substituent constants[12] at the 4′-and 5′-positions simultaneously, we selected the Pd-catalyzed Suzuki coupling reaction between organoboron compounds and organic halides. The difference between the reaction rates of iodides and bromides allows for selective coupling with the iodides even in the presence of bromides. Additionally, commercial availability of many boronic acids and the ease of obtaining various halogenated aromatic compounds make further chemical modification feasible. The synthetic strategies employed to prepare four disubstituted HBT derivatives are depicted in Scheme 1. From commercially available 3-iodophenol, 2-hydroxy-4-iodobenzaldehyde was first synthesized according to a previously reported method,[13] before bromination at the 5′-position to obtain 5-bromo-2-hydroxy-4-iodobenzaldehyde. The reaction between 5-bromo-2-hydroxy-4-iodobenzaldehyde with 2-aminothiophenol in the presence of HCl/H_2O_2 in methanol yielded 2-(benzo[*d*]thiazol-2-yl)-4-bromo-5-iodophenol, a very important intermediate, which could be readily monitored

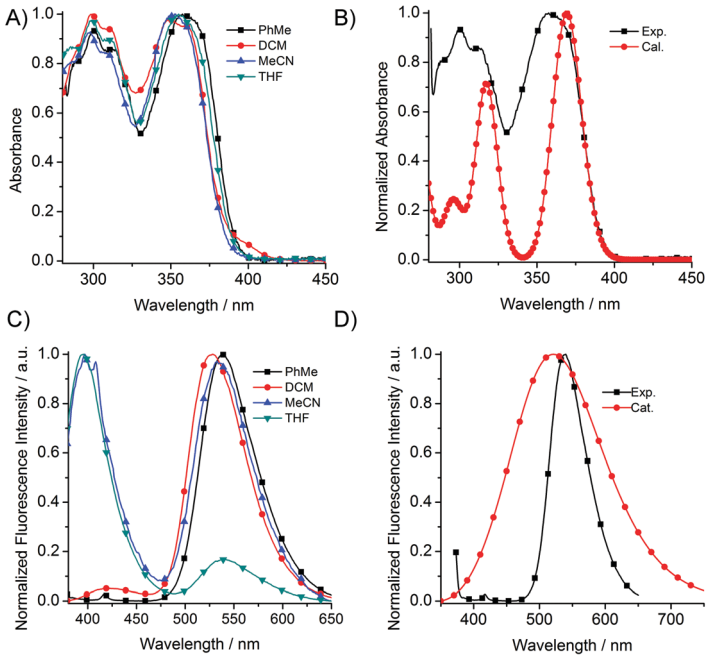

Fig. 1 (A) Absorption spectra and (C) fluorescence spectra of **HBT-H-H** in various solvents; comparison of experimentally obtained and theoretically calculated (B) absorption spectra and (D) fluorescence spectra in toluene solution.

through thin layer chromatography owing to its strong yellow fluorescence under UV irradiation. Under Suzuki reaction conditions, the reaction of this intermediate with two equivalents of either benzeneboronic acid or 4-cyanophenylboronic acid afforded a biphenyl-modified HBT derivative (**HBT-H-H**) and a bi-4-cyanophenyl-modified HBT derivative (**HBT-CN-CN**), respectively. The reaction of this intermediate with one equivalent of 4-cyanophenylboronic acid easily afforded another important intermediate, compound **4**, which was further reacted with phenylboronic acid or 4-methoxyphenylboronic acid to obtain **HBT-CN-H** and **HBT-CN-OMe**, respectively. These new compounds were unambiguously characterized by ^{1}H and ^{13}C nuclear magnetic resonance spectroscopy and high-resolution mass spectrometry (Fig. S11–S30, ESI†). Additionally, single-crystal X-ray diffraction analysis was also performed on **HBT-H-H** (CCDC 1546814).† It should be noted that this synthesis method could be readily applied in synthesizing other disubstituted or multisubstituted HBT derivatives at different sites of the parent HBT molecule.

Photophysical properties of HBT-H-H in solution and theoretical calculations

We first measured the absorption and fluorescence emission spectra of **HBT-H-H** in several solvents with different polarities and H-bonding abilities. Meanwhile, to gain a deeper insight into the electronic structures and the excited states of the enol- and keto-tautomers of **HBT-H-H**, density functional theory (DFT) calculations were also conducted.[14] As shown in Fig. 1A, the absorption spectra have similar profiles, indicating that the solvents have little effect on the absorption spectra, which is consistent with the previously reported result.[15] In toluene, there are three main absorption bands at 357 nm, 313 nm, and 300 nm, which is in good agreement with the calculated results (Fig. 1B). The vertical excitation calculations suggested that the three absorption peaks in toluene from the lowest to highest energy bands correspond to transitions from the HOMO, HOMO−1, and HOMO−2 to the LUMO of the π-systems, respectively (Table S1 and Fig. S1, ESI†).

In contrast to the absorbance, **HBT-H-H** shows remarkable solvent-dependent fluorescence (Fig. 1C), which is a characteristic feature for ESIPT dyes.[16] In the nonpolar solvent PhMe and the medium polarity solvent DCM, one dominant band with an exceedingly large Stokes shift (∼169 nm) was observed. In MeCN and THF, which can act as H-bond acceptors, well-separated dual bands were detected, one with a normal Stokes shift (∼36 nm), and the other with a larger Stokes shift (∼172 nm). This phenomenon has also been observed for other ESIPT systems.[15] We ascribe the band with the normal Stokes shift to the emission from a locally excited state (N*), and the band with the large Stokes shift to the emission from an ESIPT state (K*). To verify this, we conducted several measurements. First, the excitation spectra of **HBT-H-H** in different solvents resembled their respective absorption spectrum (Fig. S2, ESI†), which reveals that the two emission bands originate from the identical ground state of the enol-tautomer.[17] Second, as shown in Fig. 2, from the HOMO to the LUMO of the enol-tautomer, the electron density of oxygen in the phenolic hydroxyl decreases, while that of nitrogen in the benzothiazole ring increases. This change in electron density from the ground state to the excited state simultaneously improves the acidity of the phenolic hydroxyl group and the basicity of the nitrogen, allowing for proton transfer from oxygen to nitrogen to complete the tautomerization

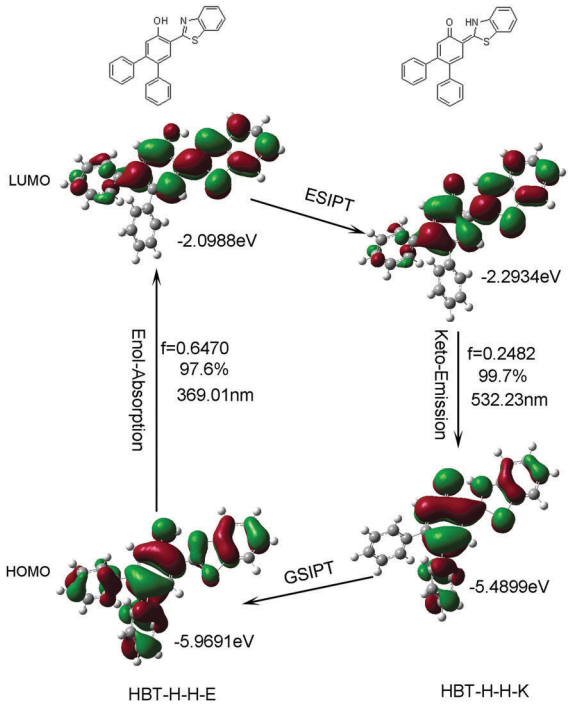

Fig. 2 Schematic representation of the four-level photophysical process for **HBT-H-H**.

from the enol- to the keto-tautomer.[18,19] Meanwhile, the more acidity of the hydroxy group and the more basicity of the nitrogen atom in the excited state are also reflected in the elongated O–H bond and the shortened N···H distance (Fig. S3, ESI†). Actually, the keto tautomer in the excited state has been detected through femtosecond transient absorption spectra.[15,20] Third, the energy levels of the HOMOs and LUMOs of the enol-tautomer and keto-tautomer were compared (Fig. 2). The LUMO of the keto-tautomer is more stable by 0.1946 eV than that of the enol-tautomer, and the HOMO of the keto-tautomer is less stable by 0.4792 eV compared to the HOMO of the enol-tautomer. Therefore, the much smaller HOMO–LUMO energy gap of the keto-tautomer than that of the enol-tautomer underpins the large Stokes shift due to keto-emission.[21] Finally, the theoretically calculated emission wavelength (532.23 nm) in PhMe based on the optimized S_1 state geometry of the keto-tautomer is very close to the experimentally observed value (537 nm) (Fig. 1D and Fig. S4, ESI†). In nonpolar or medium polarity solvents, which could not compete with the nitrogen for the phenolic hydroxyl proton, the dominant form of **HBT-H-H** is the closed enol bearing an intramolecular H-bond, with excitation resulting in sole keto-emission. In solvents that can act as an H-bond donor, intermolecular H-bonds with solvent molecules may partially or completely destroy intramolecular H-bonds. Recently, Mcgrier and coworkers have also shown that trifluoroacetic acid makes the keto emission hypsochromically shift to the enol emission in the ESIPT system. This is attributed to the protonation of the imine nitrogen atoms, which completely muffle the ESIPT process.[15] Therefore, excitation of **HBT-H-H** in H-bond donating solvents results in both enol- and keto-emission.

As shown in Fig. 2, for the keto-tautomer, the HOMO is mainly located on the phenol ring and the phenyl in the 5′-position, and has no distribution on the 4′-position phenyl. In contrast, the LUMO is on the phenol ring, the benzothiazole moiety and the 4′-position phenyl, and has no distribution on the 5′-position phenyl. Therefore, the substituents at the 5′-position have more of an effect on the HOMO, whereas the substituents at the 4′-position have more of an effect on the LUMO. It is well known that regardless of the position of the substituent, the energy levels of both the HOMO and LUMO decrease with increasing electron-withdrawing ability of the substituent group.[22] Accordingly, anchoring an electron-withdrawing substituent at the 4′-position would lead to a smaller energy gap between the HOMO and LUMO, because the decreasing magnitude of the LUMO energy level would be bigger than that of the HOMO; and the opposite effect would be observed for the substitutions at the 5′-position. The above analysis indicates that the trend of the shift of the keto-emission could be predicted by theoretical calculations.

Photophysical properties of other disubstituted HBT derivatives and theoretical calculations

In order to further study the electric effects on the photophysical properties of disubstituted HBT derivatives and to verify that the trend of the shift of the keto-emissions could be predicted by theoretical calculations, we further synthesized three disubstituted HBT derivatives, **HBT-CN-H**, **HBT-CN-OMe**, and **HBT-CN-CN** (molecular structures shown in Scheme 1 and photophysical data summarized in Table 1).

First, the fluorescence spectrum of **HBT-CN-H**, which bears an electron-withdrawing CN group at the 4′-position, was compared with that of **HBT-H-H** in different solvents. In PhMe and DCM, both the molecules solely showed keto-emission (Fig. 3A and B), and **HBT-CN-H** shows red-shifted fluorescence (from 537 to 539 nm) with increasing Φ_f (from 1.4% to 3.7%). In THF and MeCN, the intensity ratio of K* *versus* N* (I_{K^*}/I_{N^*}), an important characteristic of ESIPT, increased accordingly (Fig. 3C and D). As shown in Fig. 4, in comparison with **HBT-H-H**, the energy levels of the HOMO and LUMO of its keto-tautomer were lower by 0.1589 eV and 0.2169 eV, respectively, which results in a smaller energy gap, and is in accordance with our above conjecture. The difference of I_{K^*}/I_{N^*} indicates that the intramolecular H-bond in **HBT-CN-H** is reinforced and less likely to be undermined by solvent molecules, and that the ESIPT is promoted.[19] In the optimized ground state of the enol-tautomer of **HBT-CN-H** (Fig. 5), the N···O

Table 1 Photophysical data of the disubstituted HBT derivatives

	HBT-H-H	HBT-CN-H	HBT-CN-OMe	HBT-CN-CN
σ	0.00/0.00	0.66/0.00	0.66/−0.17	0.66/0.66
λ_{em} in PhMe (Exp.)	537	539	548	533
λ_{ex} in PhMe (Cal.)	532.23	536.72	570.62	516.23
λ_{ex} in PhMe (Exp.)	368	370	372	366
$\Delta\lambda$ in PhMe	169	169	176	167
Φ_f in PhMe (%)	1.4	3.7	2.4	8.5
Chemical shift	12.591	12.690	12.637	12.834
λ_{ex} in DCM (Exp.)	528	533	547	527

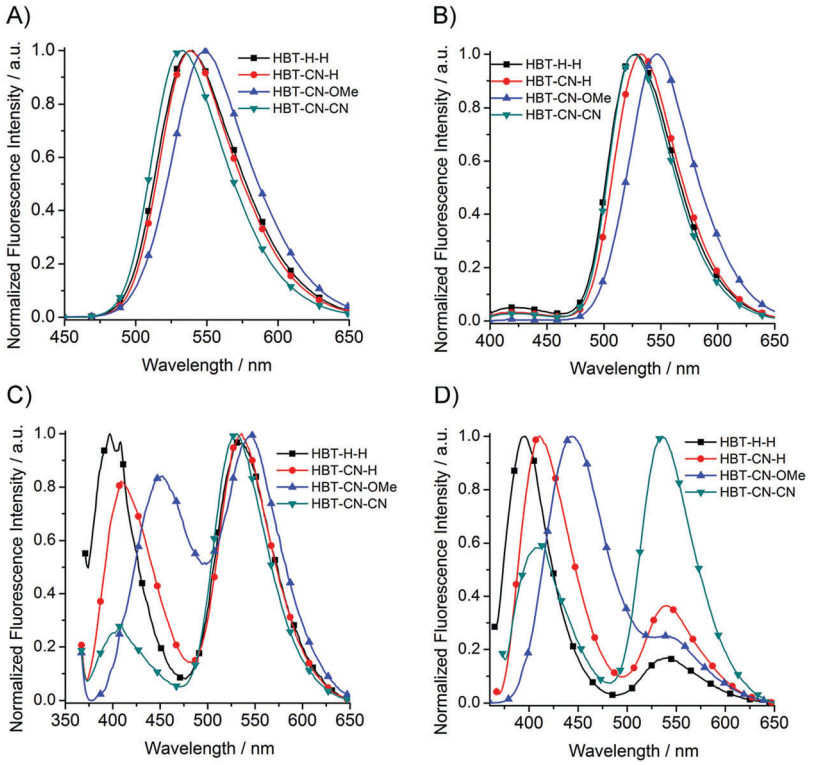

Fig. 3 Comparing fluorescence spectra of the disubstituted HBT derivatives in different solvents. (A) PhMe, (B) DCM, (C) THF, and (D) MeCN.

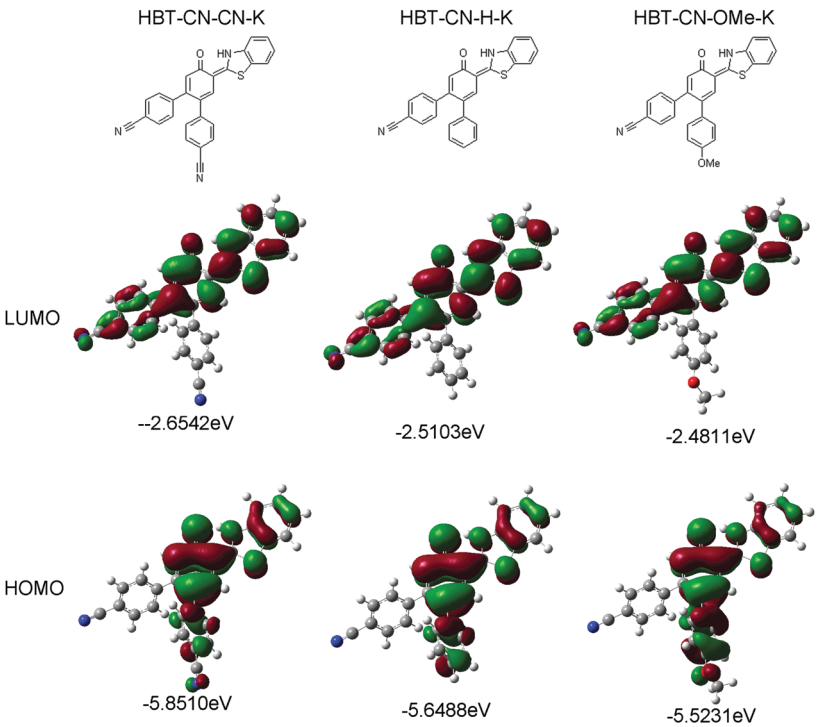

Fig. 4 DFT-calculated HOMOs and LUMOs of the keto-tautomers of the disubstituted HBT derivatives.

and N···H distances were shortened from 2.6511 to 2.6450 Å and from 1.7697 to 1.7626 Å, respectively, and the O–H bond length was also increased from 0.9938 to 0.9944 Å, all of which verified the stronger H-bond in **HBT-CN-H.** The strength of the intramolecular H-bond could also be directly reflected through the chemical shift of the phenolic hydroxyl proton in the ^{1}HNMR spectra (Fig. 6), which

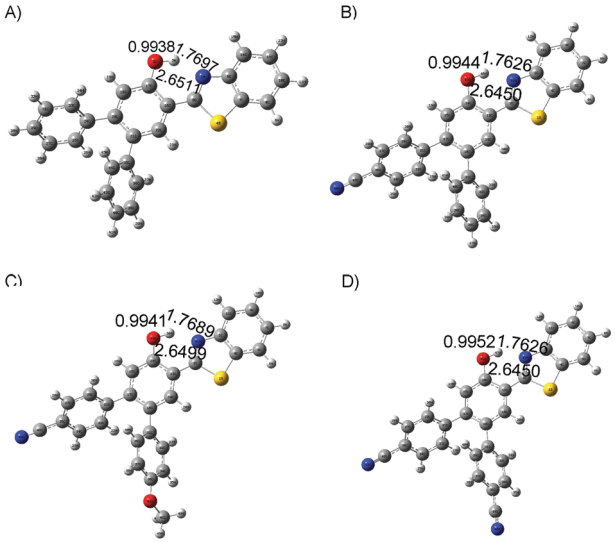

Fig. 5 The energy-optimized geometric structures of the enol-tautomer of the disubstituted HBT derivatives in the ground-state and the relevant H-bond parameters.

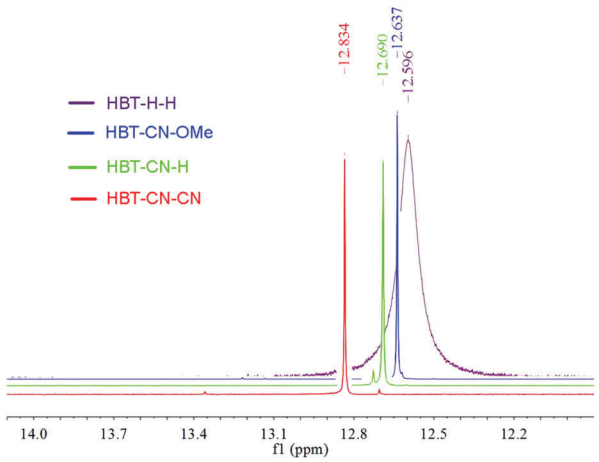

Fig. 6 The chemical shift of the phenolic hydroxyl proton of the disubstituted HBT derivatives in ^{1}H NMR ($CDCl_3$).

shifted downfield by 0.094 ppm from 12.596 to 12.690 ppm. The similar correlation was also reflected in other ESIPT dyes.[19] The improving strength of the intramolecular H-bond in **HBT-CN-H** also explains its higher Φ_f, because for ESIPT fluorophores, H-bond strength is often positively correlated with Φ_f.[23] Therefore, introducing electron-withdrawing groups at the 4′-position of HBT not only red-shifts the fluorescence emission, but also improves the Φ_f.

Fixing an electron-withdrawing group like CN at the 4′-position of HBT, we continued to study the substituent effect at the 5′-position, and introduced an electron-donating group (OMe) and an electron-withdrawing group (CN), respectively, to obtain **HBT-CN-OMe** and **HBT-CN-CN**. As shown in Fig. 3A and B, in comparison with **HBT-CN-H**, **HBT-CN-OMe** showed a red-shifted keto-emission (from 539 to 548 nm) and a reduced Φ_f (from 3.7% to 2.4%), whereas **HBT-CN-CN** showed a blue-shifted keto-emission (from 539 to 533 nm) and an enhanced Φ_f (from 3.7% to 8.5%). Additionally, **HBT-CN-OMe** demonstrated a lower I_{K^*}/I_{N^*}, and **HBT-CN-CN** demonstrated a higher ratio, which indicates that the electron-withdrawing group in **HBT-CN-CN** reinforced the H-bond, while the electron-donating group in **HBT-CN-OMe** weakened the H-bond. The calculated HOMO/LUMO energy levels of **HBT-CN-CN** were −5.8510/−2.6542 eV, which are lower than those of **HBT-CN-H** (−5.6488/−2.5103 eV) (Fig. 4). In contrast, the HOMO/LUMO energy levels (−5.5231/−2.4811 eV) of **HBT-CN-OMe** are higher than those of **HBT-CN-H** (Fig. 4). These results can be explained by the fact that for their keto-tautomers, the HOMOs are spread on the 5′-position phenyls, and have no distributions on the 4′-position phenyls, while the distribution of the LUMOs is opposite to that of the HOMOs. Therefore, the substituents at the 5′-position dramatically affect the HOMOs. The electron-withdrawing group at the 5′-position simultaneously lowers the energy levels of the LUMO and HOMO; the decreasing magnitude of the LUMO is smaller than that of the HOMO, which results in a bigger energy gap, and consequently, blue-shifted fluorescence emission. While the electron-donating group at the 5′-position simultaneously elevates the energy levels of the LUMO and the HOMO, the increasing magnitude of the LUMO energy level is smaller than that of the HOMO, resulting in a smaller energy gap and consequent red-shifted fluorescence emission. As expected, the trend of the HOMO–LUMO energy gap is **HBT-CN-CN** > **HBT-CN-H** > **HBT-CN-OMe**, which is in line with the experimental data. In the optimized ground state of enol-tautomers for **HBT-CN-OMe** (Fig. 5), the distances of N···O and N···H were elongated from 2.6450 to 2.6499 Å and from 1.7626 to 1.7689 Å, respectively, while the bond length of OH was shortened from 0.9944 to 0.9941 Å. For **HBT-CN-CN**, although the distances of N···O and N···H did not change, the OH bond length was increased by 0.008 Å from 0.9944 to 0.9952 Å. The change in strength of the H-bond could also be deduced from the chemical shift of the phenolic hydroxyl proton in the respective ^{1}H NMR spectrum (Fig. 6). For **HBT-CN-CN** the proton downshifts by 0.144 ppm, while for **HBT-CN-OMe** the proton upshifts by 0.053 ppm. Therefore, the trend of H-bond strength is **HBT-CN-CN** > **HBT-CN-H** > **HBT-CN-OMe**, which is in line with the changing trend of Φ_f. It should be noted that all the resonance signals of OH appeared significantly downfield at δ > 12 ppm for these HBT derivatives, clearly indicating strong H-bond formation in these compounds and guaranteeing the occurrence of keto-emission.[24] In general, the theoretical calculations agree well with the experimentally observed trends.

Photophysical properties of HBT-H-H in the crystalline state

Yellow single crystals of **HBT-H-H** suitable for single-crystal X-ray diffraction analysis were obtained by slow evaporation of DCM from the solution at room temperature. Suitable crystals of other compounds could not be obtained. Crystals of **HBT-H-H** emitted strong yellow fluorescence under UV light irradiation, which prompted us to study the solid-state photophysical properties of **HBT-H-H**. Solid-state fluorescence spectroscopy showed that the maximum emission wavelength shifted bathochromically by 8 nm (Fig. S8, ESI†), and the Φ_f and τ were

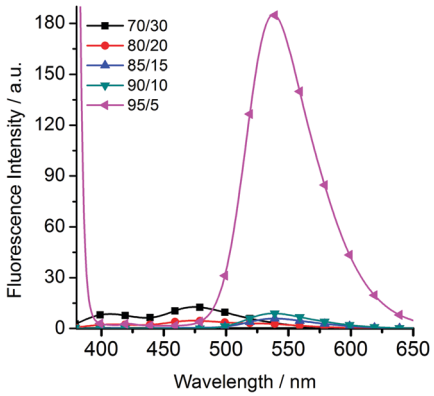

Fig. 7 Fluorescence spectra changes of **HBT-H-H** depending on the water fractions in THF.

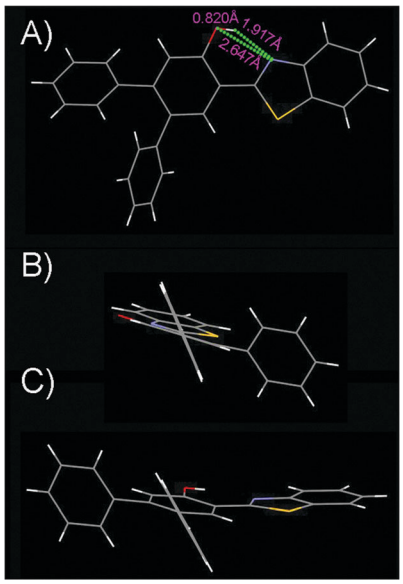

Fig. 8 (A) View of the intramolecular H-bonding interaction of the **HBT-H-H** crystal; the distorted angle between the phenol and the phenyl ring (B) at the 4′- position and (C) at the 5′- position.

49.63% and 4.8181 ns, 35.45-fold and 8.6-fold higher than those measured in toluene solution, respectively (Fig. S9 and S10, ESI†).

Additionally, the fluorescence spectra of **HBT-H-H** in the THF/H_2O systems were also measured, as **HBT-H-H** is soluble in THF but not in water. The results demonstrated that the fluorescence intensity gradually increased with increasing volume fraction of water in the mixtures from 70% to 90% and suddenly improved at 95% (Fig. 7).[25] Consequently, this HBT derivative is an AIE-active dye and the nonradiative deactivation pathway was efficiently suppressed in the aggregated state.

It is well known that the molecular spatial configuration plays a vital role in determining the stacking mode of a dye molecule and thus affects the photophysical properties of the molecule in the resultant aggregated state.[26] The crystal data are presented in Table S2 (ESI†), and the crystal structure of **HBT-H-H** is shown in Fig. 8. **HBT-H-H** crystallizes in the triclinic space group $P\bar{1}$. **HBT-H-H** adopts a propeller-shaped conformation and is not a planar molecule. In the four planar π-units, the phenol and benzothiazole rings are coplanar with a mere 5.53° dihedral angle because of the existence of relatively strong intramolecular six-membered-ring H-bonds. The dihedral angles between the phenol and the adjacent phenyl rings at the 4′- and 5′-positions are 50.2° and 50.9°, respectively, which were caused by the steric effect of biphenyl in the *ortho*-positions.[27] It should be noted that although the O–H bond length is shortened by 0.1738 Å and the H···N distance is increased by 0.1473 Å when moving from the solution state to the crystalline state, the overall intramolecular H-bond distance between O···N is shortened by 0.004 Å from 2.651 to 2.647 Å. Therefore, the strength of the intramolecular H-bond was reinforced in the crystalline state, which facilitated the proton transfer from oxygen to nitrogen *via* intramolecular H-bonding.

The restricted intramolecular motion is another central factor in the improvement of Φ_f in the crystalline state.[28] The packing diagrams of **HBT-H-H** are shown in Fig. 9. Though the two phenyls are not coplanar with the phenol ring, the coplanar HBT moieties of the neighboring molecules are still parallel, which have two kinds of intermolecular π–π stacking, one distance is 3.510 Å, the other is 3.660 Å, both of which are relatively larger than the characteristic distance in the crystal stacking of the planar π-conjugated systems. Additionally, two kinds of C–H···π hydrogen bonds are also formed. One bond with a distance of 2.891 Å is formed between the hydrogen atom

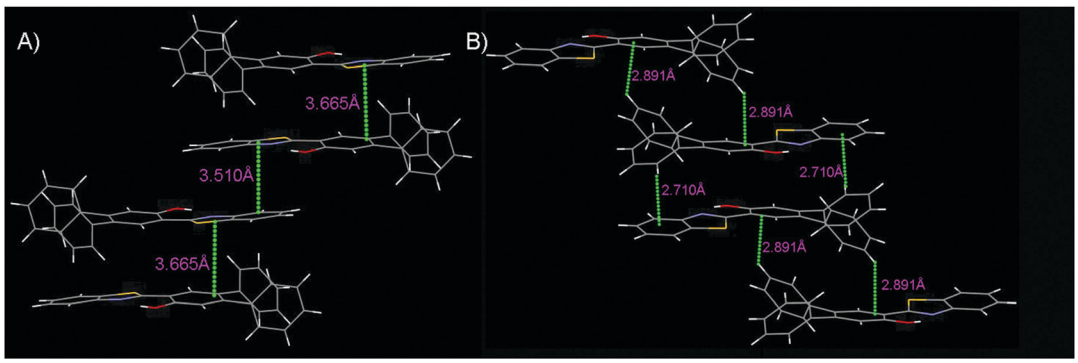

Fig. 9 (A) Two kinds of intermolecular π–π stacking in the **HBT-H-H** crystal; (B) two kinds of C–H···π hydrogen bonds in the **HBT-H-H** crystal.

of the 5′-position phenyl ring and the π-cloud of the phenol ring. The other bond, with a distance of 2.710 Å, is formed between the hydrogen atoms of the 4′-position phenyl ring and the π-cloud of the phenyl ring in the benzothiazole moiety. These weak forces help rigidify its conformation and hamper the free rotation of the C–C σ bond between the phenyl ring and the phenol ring.[29] As a result, the excited state energy loss *via* the nonradiative relaxation channel is dramatically reduced, which makes the molecules emit intensively in the crystalline phase.

Conclusion

We have designed and synthesized four disubstituted HBT derivatives through Suzuki coupling. TD-DFT calculations reveal that the maximum absorption band of **HBT-H-H** is attributed to the HOMO → LUMO transition of its enol-tautomer, and its maximum emission band is attributed to the LUMO → HOMO relaxation of its keto-tautomer. The HOMOs distribute more on the 5′-position phenyl, and the LUMOs more on the 4′-position phenyl. Thus, the electronic effect of substituents at the 5′-position is opposite to that at the 4′-position. The experimentally observed results are in agreement with the theoretical calculations. Therefore, the shifting trends of keto-emission could be predicted by theoretical calculations, which would provide valuable information for designing other high-performance ESIPT dyes by modifying the molecular structures. Additionally, these derivatives show highly efficient keto-emission in the crystalline state. X-ray analysis indicates that the easier proton transfer through stronger intramolecular H-bonds and the restriction of the free rotation of biphenyl rings *via* aggregate formation are responsible for this AIE.

Experimental

Materials

3-Iodophenol, phenylboronic acid, 4-cyanophenylboronic acid, 4-methoxyphenylboronic acid, 2-aminothiophenol and $PdCl_2(PPh_3)_2$ were purchased from Energy Chemical (Shanghai, China). All other materials were purchased from local commercial suppliers and were of analytical reagent grade, unless otherwise stated. Solvents were purified by standard procedures. Ultrapurified water was supplied by a Milli-Q system (Millipore). All the reactions were monitored by thin-layer chromatography (TLC) with detection by UV.

Instruments

The ^{1}H and ^{13}C NMR spectra of the products were recorded on a Bruker 500 MHz NMR spectrometer in $CDCl_3$ solution using tetramethylsilane (TMS) as the internal standard, and chemical shifts were given in ppm and coupling constants (J) in Hz. High resolution mass spectra (HRMS) were recorded on a Thermo Scientific LTQ Orbitrap XL using standard conditions (electron spray ionization, ESI). The UV absorption spectra were obtained on a UV-vis spectrophotometer (U-3310). The fluorescence spectra were recorded on a fluorospectrophotometer (F-7000). The fluorescence quantum yield (Φ_f) in the solution was determined by using quinine sulfate (Φ_f = 0.55 in 0.1 M H_2SO_4) as a standard.

Computational methods

All the calculations were performed using the Gaussian 09 package. To evaluate the solvent effect, toluene was employed as the solvent in a self-consistent reaction field calculation using a polarized continuum model. The ground state (S_0) and the first singlet excited state (S_1) geometries of the enol and keto tautomers of these HBT-based disubstituted derivatives were optimized using density functional theory (DFT) and time-dependent density functional theory (TDDFT) at the B3LYP/6-31+G(d) level, respectively. The UV-vis absorption of **HBT-H-H** (vertical excitation) was calculated with the TDDFT method based on the optimized S_0 state geometry of the enol tautomer. For the keto emission, the emission wavelengths were calculated based on the S_1 optimized geometries of the keto tautomers.

Crystal structural determination

The single crystals of compound **HBT-H-H** were obtained by the slow diffusion of CH_2Cl_2 from solution for several days at room temperature. A single crystal of **HBT-H-H** with dimensions of 0.40 × 0.30 × 0.20 mm was selected. The lattice constants and diffraction intensities were measured at room temperature on a Bruker SMART APEX-II CCD area detector using graphite-monochromated Mo Kα radiation (λ = 0.71073 Å). Data reduction and integration were done by the INTEGRATE program of the APEX2 software. The semi-empirical absorption correction was applied using the SCALE program. The structure was solved by direct methods and refined by the full matrix least-squares method on F^2 using SHELX.

Synthesis and characterization

2-Hydroxy-4-iodobenzaldehyde (Compound 1). Compound **1** was synthesized according to the previously reported method.[13] ^{1}H NMR (500 MHz, $CDCl_3$) δ 11.06 (s, 1H), 9.89 (s, 1H), 7.48 (s, 1H), 7.44 (dd, J = 8.1, 1.4 Hz, 1H), 7.28 (d, J = 8.1 Hz, 1H).

5-Bromo-2-hydroxy-4-iodobenzaldehyde (Compound 2). To a solution of Compound **1** (20 mmol, 4.96 g) in 50 mL of acetic acid was added bromine (20 mmol, 1.04 mL). The reaction mixture was stirred at room temperature overnight. After that, more Br_2 (0.2 equiv., 0.2 mL) was added and allowed to react for another 12 h. The saturated solution of $Na_2S_2O_3$ was added until the color of Br_2 disappeared, and the mixture was extracted with CH_2Cl_2 (100 mL × 2). The combined organic layers were washed with brine and water, dried over $MgSO_4$ and concentrated. The residue was purified by flash chromatography on silica gel to afford the targeted product as a pale-yellow powder (3.99 g, 64%). ^{1}H NMR (500 MHz, $CDCl_3$) δ 10.85 (s, 1H), 9.85 (s, 1H), 7.78 (s, 1H), 7.66 (s, 1H). ^{13}C NMR (126 MHz, $CDCl_3$) δ 195.09, 159.38, 135.50, 130.13, 121.65, 119.37, 112.28.

2-(Benzo[*d*]thiazol-2-yl)-4-bromo-5-iodophenol (Compound 3). Compound **2** (600 mg, 1.84 mmol) was added to DMSO (1.5 mL). Under N_2 atmosphere, 2-aminothiophenol (236 μL, 2.2 mmol) was added and the resulting mixture was refluxed for 2 h. The reaction was cooled to RT. The crude solution was extracted

with dichloromethane, and the combined organic layer was washed with water and dried over $MgSO_4$ and the solvent was evaporated *in vacuo*. The residue was further purified by column chromatography (PE/DCM, 5/1) to give the targeted product as a yellow solid. Yield: 594 mg, 75%. ^{1}H NMR (500 MHz, $CDCl_3$) δ 12.60 (s, 1H), 8.05 (d, J = 8.0 Hz, 1H), 7.98 (d, J = 8.0 Hz, 1H), 7.91 (s, 1H), 7.72 (s, 1H), 7.59 (m, 1H), 7.51 (m, 1H). ^{13}C NMR (126 MHz, $CDCl_3$) δ 167.15, 156.55, 151.55, 132.47, 130.44, 129.75, 127.12, 126.21, 122.47, 121.70, 118.67, 118.39, 105.24.

HBT-H-H. Under N_2 atmosphere, Compound **3** (200 mg, 0.46 mmol), phenylboronic acid (226 mg, 1.8 mmol), K_2CO_3 (160 mg, 1.15 mmol), and $PdCl_2(PPh_3)$ (5/100 equiv., 16 mg) were added to a solution of dioxane/H_2O (8 mL/2 mL). The resulting solution was refluxed for 14 h. The reaction mixture was then partitioned between CH_2Cl_2 and water, and the aqueous phase was extracted with CH_2Cl_2 twice. The combined organic layer was evaporated, and the residue was purified by flash column chromatography (PE/DCM, 3/1) to give the targeted product as a yellow solid (148 mg, 85%). HRMS (ESI) m/z calcd for $C_{25}H_{18}NOS^+$ $(M + H)^+$ 380.11036, found 380.11078. ^{1}H NMR (500 MHz, $CDCl_3$) δ 12.60 (s, 1H), 8.07 (d, J = 8.0 Hz, 1H), 7.97 (d, J = 8.0 Hz, 1H), 7.77 (s, 1H), 7.58 (m, 1H), 7.47 (m, 1H), 7.30–7.27 (m, 6H), 7.25 (s, 1H), 7.24–7.21 (m, 4H). ^{13}C NMR (126 MHz, $CDCl_3$) δ 168.98, 157.09, 151.97, 145.26, 140.50, 132.65, 130.38, 129.95, 129.66, 128.03, 127.18, 126.80, 126.57, 125.62, 122.25, 121.63, 119.63, 116.02.

Compound 4. Under N_2 atmosphere, Compound **3** (600 mg, 1.4 mmol), 4-cyanobenzeneboronic acid (205 mg, 1.4 mmol), K_2CO_3 (425 mg, 3.1 mmol), and $PdCl_2(PPh_3)$ (5/100 equiv., 49 mg) were added to a solution of dioxane/H_2O (20 mL/5 mL). The resulting solution was refluxed for 14 h. The resulting solution was refluxed for 14 h. The reaction mixture was then partitioned between CH_2Cl_2 and water, and the aqueous phase was extracted with CH_2Cl_2 twice. The combined organic layer was evaporated, and the residue was purified by flash column chromatography (PE/DCM, 5/4) to give the targeted product (342 mg, 60%) as a yellow solid. MS (ESI) m/z calcd for $C_{20}H_{10}BrN_2OS^-$ $(M - H)^-$ 406.98, found 406.95. ^{1}H NMR (500 MHz, $CDCl_3$) δ 12.68 (s, 1H), 8.08 (d, J = 8.0 Hz, 1H), 8.02 (s, 1H), 8.00 (d, J = 8.0 Hz, 1H), 7.80 (d, J = 8.5 Hz, 2H), 7.67–7.55 (m, 4H), 7.52 (m, 1H), 7.13 (s, 1H). ^{13}C NMR (126 MHz, $CDCl_3$) δ 167.10, 157.13, 151.66, 144.62, 144.28, 132.71, 132.37, 131.98, 130.06, 127.14, 126.22, 122.52, 121.74, 120.36, 118.65, 118.30, 112.09, 110.74.

HBT-CN-H. Under N_2 atmosphere, Compound **4** (200 mg, 0.49 mmol), phenylboronic acid (72 mg, 0.59 mmol), K_2CO_3 (149 mg, 1.08 mmol), and $PdCl_2(PPh_3)$ (5/100 equiv., 17 mg) were added to a solution of dioxane/H_2O (8 mL/4 mL). The resulting solution was refluxed for 14 h. The reaction mixture was then partitioned between CH_2Cl_2 and water, and the aqueous phase was extracted with CH_2Cl_2 twice. The combined organic layer was evaporated, and the residue was purified by flash column chromatography (PE/DCM, 2/5) to give the targeted product as a yellow solid (158 mg, 80%). HRMS (ESI) m/z calcd for $C_{26}H_{17}N_2OS^+$ $(M + H)^+$ 405.10561, found 405.10568. ^{1}H NMR (500 MHz, $CDCl_3$) δ 12.69 (s, 1H), 8.09 (d, J = 8.0 Hz, 1H), 7.98 (d, J = 7.5 Hz, 1H), 7.79 (s, 1H), 7.60 (t, J = 6.5 Hz, 1H), 7.57 (d, J = 8.0 Hz, 2H), 7.50 (t, J = 8.0 Hz, 1H), 7.34–7.32 (m, 5H), 7.22 (s, 1H), 7.18–7.16 (m, 2H). ^{13}C NMR (126 MHz, $CDCl_3$) δ 168.53, 157.22, 151.86, 145.30, 142.89, 139.70, 132.74, 132.44, 131.84, 130.57, 130.35, 129.89, 128.39, 127.02, 125.89, 122.37, 121.68, 119.46, 118.82, 116.89, 110.96.

HBT-CN-OMe. Under N_2 atmosphere, Compound **4** (103 mg, 0.24 mmol), 4-methoxybenzeneboronic acid (36.5 mg, 0.24 mmol), K_2CO_3 (76 mg, 0.56 mmol), and $PdCl_2(PPh_3)$ (5/100 equiv., 8.5 mg) were added to a solution of dioxane/H_2O (8 mL/2 mL). The resulting solution was refluxed for 14 h. The reaction mixture was then partitioned between CH_2Cl_2 and water, and the aqueous phase was extracted with CH_2Cl_2 twice. The combined organic layer was evaporated, and the residue was purified by flash column chromatography (PE/DCM, 4/5) to give the targeted product as a yellow solid (78 mg, 75%). HRMS (ESI) m/z calcd for $C_{27}H_{19}N_2O_2S^+$ $(M + H)^+$ 435.11617, found 435.11618. ^{1}H NMR (500 MHz, $CDCl_3$) δ 12.64 (s, 1H), 8.08 (d, J = 8.0 Hz, 1H), 7.97 (d, J = 8.0 Hz, 1H), 7.76 (s, 1H), 7.60–7.56 (m, 3H), 7.50 (m, 1H), 7.34 (d, J = 8.5 Hz, 2H), 7.19 (s, 1H), 7.07 (d, J = 9.0 Hz, 2H), 6.86 (d, J = 9.0 Hz, 2H), 3.86 (s, 3H). ^{13}C NMR (126 MHz, $CDCl_3$) δ 168.58, 158.74, 156.97, 151.87, 145.49, 142.84, 132.74, 132.16, 131.78, 130.94, 130.40, 126.94, 125.86, 122.36, 121.67, 119.40, 116.87, 113.83, 55.31.

HBT-CN-CN. Under N_2 atmosphere, Compound **4** (210 mg, 0.48 mmol), 4-cyanobenzeneboronic acid (279 mg, 1.9 mmol), K_2CO_3 (224 mg, 2.2 mmol), and $PdCl_2(PPh_3)_2$ (5/100 equiv., 17 mg) were added to a solution of dioxane/H_2O (8 mL/2 mL). The resulting solution was refluxed for 14 h. The reaction mixture was then partitioned between CH_2Cl_2 and water, and the aqueous phase was extracted with CH_2Cl_2 twice. The combined organic layer was evaporated, and the residue was purified by flash column chromatography (PE/DCM, 3/5) to give the targeted product (154 mg, 75%) as a yellow solid. HRMS (ESI) m/z calcd for $C_{27}H_{16}N_3OS^+$ $(M + H)^+$ 430.10086, found 430.10101. ^{1}H NMR (500 MHz, $CDCl_3$) δ 12.83 (s, 1H), 8.10 (d, J = 8.0 Hz, 1H), 8.00 (d, J = 8.0 Hz, 1H), 7.76 (s, 1H), 7.65–7.59 (m, 5H), 7.52 (t, J = 7.7 Hz, 1H), 7.32–7.28 (m, 4H), 7.24 (s, 1H). ^{13}C NMR (126 MHz, $CDCl_3$) δ 167.99, 158.03, 151.76, 144.52, 142.77, 132.65, 132.16, 130.62, 130.19, 127.14, 126.15, 122.48, 121.73, 120.01, 118.54, 117.18, 111.60, 110.94.

Acknowledgements

This study was supported by the National Natural Science Foundation of China (21405122), and the Natural Science Foundation of Shaanxi (2016JM2009).

Notes and references

1 (*a*) A. P. Demchenko, K. C. Tang and P. T. Chou, *Chem. Soc. Rev.*, 2013, **42**, 1379; (*b*) J. Zhao, S. Ji, Y. Chen, H. Guo and P. Yang, *Phys. Chem. Chem. Phys.*, 2012, **14**, 8803; (*c*) J. E. Kwon and S. Y. Park, *Adv. Mater.*, 2011, **23**, 3615.

2 (*a*) Q. Wang, L. Xu, Y. Niu, Y. Wang, M. S. Yuan and Y. Zhang, *Chem. – Asian J.*, 2016, **11**, 3454; (*b*) Q. Wang, L. Xu, Y. Niu, Y. Wang, M.-S. Yuan and Y. Zhang, *Dyes Pigm.*, 2017, **142**, 365; (*c*) L. Xu, Q. Wang and Y. Zhang, *Dyes Pigm.*, 2017, **136**, 732.

3 (*a*) P. F. Barbara, L. E. Brus and P. M. Rentzepis, *J. Am. Chem. Soc.*, 1980, **11**, 5631; (*b*) M. Barbatti, A. J. Aquino, H. Lischka, C. Schriever, S. Lochbrunner and E. Riedle, *Phys. Chem. Chem. Phys.*, 2009, **11**, 1406.

4 J. E. Kwon, S. Park and S. Y. Park, *J. Am. Chem. Soc.*, 2013, **135**, 11239.

5 (*a*) H. Wang, W. Lin, K. P. Fritz, G. D. Scholes, M. A. Winnik and I. Manners, *J. Am. Chem. Soc.*, 2007, **129**, 12924; (*b*) L. Xiong, J. Feng, R. Hu, S. Wang, S. Li, Y. Li and G. Yang, *Anal. Chem.*, 2013, **85**, 4113; (*c*) K. Y. Chen and J. W. Hu, *J. Lumin.*, 2015, **159**, 171.

6 (*a*) Z. Wang, F. H. Yang and R. T. Yang, *J. Phys. Chem. C*, 2010, **114**, 1601; (*b*) M. Ikegami and T. Arai, *J. Chem. Soc., Perkin Trans.*, 2002, **2**, 1296.

7 (*a*) J. Ma, J. Zhao, P. Yang, D. Huang, C. Zhang and Q. Li, *Chem. Commun.*, 2012, **48**, 9720; (*b*) P. Yang, J. Zhao, W. Wu, X. Yu and Y. Liu, *J. Org. Chem.*, 2012, **77**, 6166.

8 D. Yao, S. Zhao, J. Guo, Z. Zhang, H. Zhang, Y. Liu and Y. Wang, *J. Mater. Chem.*, 2011, **21**, 3568.

9 J. Cheng, D. Liu, L. Bao, K. Xu, Y. Yang and K. Han, *Chem. – Asian J.*, 2014, **9**, 3215.

10 T. I. Kim, H. J. Kang, G. Han, S. J. Chung and Y. Kim, *Chem. Commun.*, 2009, 5895.

11 (*a*) Z. Ning, Z. Chen, Q. Zhang, Y. Yan, S. Qian, Y. Cao and H. Tian, *Adv. Funct. Mater.*, 2007, **17**, 3799; (*b*) Z. Zhao, S. Chen, C. Deng, J. W. Y. Lam, C. Y. K. Chan, P. Lu, Z. Wang, B. Hu and X. Chen, *J. Mater. Chem.*, 2011, **21**, 10949.

12 E. L. Eliel, S. H. Wilen and L. N. Mander, *Chem. Rev.*, 1991, **91**, 165.

13 H. Yin, B. Zhang, H. Yu, L. Zhu, Y. Feng, M. Zhu, Q. Guo and X. Meng, *J. Org. Chem.*, 2015, **80**, 4306.

14 G. J. Zhao, J. Y. Liu, L. C. Zhou and K. L. Han, *J. Phys. Chem. B*, 2007, **111**, 8940.

15 P. Jagadesean, T. Whittemore, T. Beirl, C. Turro and P. Mcgrier, *Chem. – Eur. J.*, 2017, **23**, 917.

16 (*a*) J. Seo, S. Kim and S. Y. Park, *J. Chem. Soc.*, 2004, **126**, 11154; (*b*) L. Xie, Y. Chen, W. Wu, H. Guo, J. Zhao and X. Yu, *Dyes Pigm.*, 2012, **92**, 1361; (*c*) K. Benelhadj, W. Muzuzu, J. Massue, P. Retailleau, A. Charaf-Eddin, A. D. Laurent, D. Jacquemin, G. Ulrich and R. Ziessel, *Chem. – Eur. J.*, 2014, **20**, 12843.

17 X. Zhang and J.-Y. Liu, *Dyes Pigm.*, 2016, **125**, 80–88.

18 (*a*) G. Granucci, J. T. Hynes and T. H. Tranthi, *J. Am. Chem. Soc.*, 2000, **122**, 12243; (*b*) W. Bartok, P. J. Lucchesi and N. S. Snider, *J. Am. Chem. Soc.*, 2002, **84**, 1842.

19 G. Ding, Y. Lu, Y. Gong, L. Ma, Z. Luo, S. Zhang, F. Gao and H. Li, *Tetrahedron*, 2016, **72**, 3040.

20 C. L. Chen, H. W. Tseng, Y. A. Chen, J. Q. Liu, C. M. Chao, K. M. Liu, T. C. Lin, C. H. Hung and Y. L. Chou, *J. Phys. Chem. A*, 2016, **120**, 1020.

21 L. Xie, Y. Chen, W. Wu, H. Guo, J. Zhao and X. Yu, *Dyes Pigm.*, 2012, **92**, 1361.

22 (*a*) S. Dey, A. Efimov, C. Giri, K. Rissanen and H. Lemmetyinen, *Eur. J. Org. Chem.*, 2011, 6226; (*b*) Y. Qin, I. Kiburu and A. Shimul Shah, *Org. Lett.*, 2006, **8**, 5227; (*c*) F. Qi, J. Lin, X. Wang, P. Cui, H. Yan, S. Gong, C. Ma, Z. Liu and W. Huang, *Dalton Trans.*, 2016, **45**, 7278.

23 (*a*) K. Sakai, S. Takahashi, A. Kobayashi, T. Akutagawa, T. Nakamura, M. Dosen, M. Kato and U. Nagashima, *Dalton Trans.*, 2010, **39**, 1989; (*b*) K.-i. Sakai, H. Kawamura, N. Kobayashi, T. Ishikawa, C. Ikeda, T. Kikuchi and T. Akutagawa, *CrystEngComm*, 2014, **16**, 3180.

24 (*a*) T.-C. Fang, H.-Y. Tsai, M.-H. Luo, C.-W. Chang and K.-Y. Chen, *Chin. Chem. Lett.*, 2013, **24**, 145; (*b*) G. P. Moloney, R. W. Gable, M. N. Iskander, D. J. Craik and M. F. Mackay, *Aust. J. Chem.*, 1990, **43**, 99.

25 (*a*) H. G. Lu, Y. D. Zheng, X. W. Zhao, L. J. Wang, S. Q. Ma, X. Q. Han, B. Xu, W. J. Tian and H. Gao, *Angew. Chem., Int. Ed.*, 2016, **55**, 155; (*b*) Y. Qian, S. Y. Li, G. Q. Zhang, Q. Wang, S. Q. Wang, H. J. Xu, C. Z. Li, Y. Li and G. Q. Yang, *J. Phys. Chem. B*, 2007, **111**, 5861.

26 (*a*) M.-S. Yuan, D.-E. Wang, P. Xue, W. Wang, J.-C. Wang, Q. Tu, Z. Liu, Y. Liu, Y. Zhang and J. Wang, *Chem. Mater.*, 2014, **26**, 2467; (*b*) Z. Zhang, B. Xu, J. Su, L. Shen, Y. Xie and H. Tian, *Angew. Chem.*, 2011, **50**, 11654.

27 F. Qi, J. Lin, X. Wang, P. Cui, H. Yan, S. Gong, C. Ma, Z. Liu and W. Huang, *Dalton Trans.*, 2016, **45**, 7278.

28 (*a*) J. Luo, Z. Xie, J. W. Y. Lam, L. Cheng, H. Chen, C. Qiu, H. S. Kwok, X. Zhan, Y. Liu, D. Zhu and B. Z. Tang, *Chem. Commun.*, 2001, 1740; (*b*) Y. Hong, J. W. Lam and B. Z. Tang, *Chem. Commun.*, 2009, 4332; (*c*) J. Liu, J. W. Lam and B. Z. Tang, *Chem. Rev.*, 2009, **109**, 5799.

29 (*a*) X. Q. Wang, Q. S. Liu, H. Yan, Z. P. Liu, M. G. Yao, Q. F. Zhang, S. W. Gong and W. J. He, *Chem. Commun.*, 2015, **46**, 7497; (*b*) J. Mei, Y. Hong, J. W. Y. Lam, A. Qin, Y. Tang and B. Z. Tang, *Adv. Mater.*, 2014, **26**, 5429.

